Chemical Physics Letters 724 (2019) 42–49

Contents lists available at ScienceDirect

Chemical Physics Letters

journal homepage: www.elsevier.com/locate/cplett

Research paper

Enhanced morphology and photoelectric properties of one-dimensional TiO_2 nanorod array films

Yafeng Deng[a], Zhanhong Ma[a], Fengzhang Ren[a,b,*], Guangxin Wang[a,c], Alex A. Volinsky[d]

[a] School of Materials Science and Engineering, Henan University of Science and Technology, Luoyang 471023, PR China
[b] Henan Collaborative Innovation Centre of Non-Ferrous Generic Technology, Luoyang 471023, PR China
[c] Henan Key Laboratory of Non-Ferrous Materials Science & Processing Technology, Luoyang 471023, PR China
[d] Department of Mechanical Engineering, University of South Florida, Tampa, FL 33620, USA

HIGHLIGHTS

- 1D TNA films with ideal morphology were prepared by the two-step process.
- The optical performance of 1D TNA films was enhanced by narrowing the bandgap.
- The 1D TNA films achieved efficient charge separation with higher photocurrent density.

ARTICLE INFO

Keywords:
One-dimensional TiO_2 nanorod array films
Two-step process
TiO_2 compact layer
Hydrothermal reaction time

ABSTRACT

One-dimensional TiO_2 nanorod array films (1D TNA films) were prepared by the two-step process. The results show that the density of 1D TNA films is significantly improved with the presence of TiO_2 compact layer (TCL) and the hydrothermal reaction time of 15 h. The TiO_2 crystallinity is improved. The utilization efficiency of the visible light is increased with the lower concentration of crystal defects. The charge recombination center caused by the defects decreased, while the electrons and holes were effectively separated, thus the charge recombination rate was lowered, and better charge transport performance caused the transient photocurrent to increase significantly.

1. Introduction

Nano-scale ultra-fine TiO_2 has become one of the international research hotspots because of its unique semiconductor properties and broad application prospects [1,2]. As a semiconductor material, nano-TiO_2 not only has high refractive index, high visible light transmittance, large dielectric constant and stable chemical properties, but it also has excellent photoelectricity [3], gas sensitivity [4], photocatalysis [5] and electrochromism [6], along with other properties. It is widely used in new solar cells [7,8], gas sensors [9], as photocatalytic material [10], and in other fields. Among them, one-dimensional nano-TiO_2 is a typical representative TiO_2 material, which has been studied a lot. At present, the ways to prepare one-dimensional TiO_2 nanomaterials include hydrothermal [11,12], anodizing [13,14], and template [15] methods. Among them, the hydrothermal method is the most commonly used. On the one hand, the hydrothermal method can directly grow one-dimensional TiO_2 nanostructured materials on a conductive substrate, eliminating the complicated preparation process of other methods, and obtaining nano-array films with good orientation. Moreover, the one-dimensional TiO_2 nanomaterial is firmly bonded to the substrate, which is better for later processing and use. On the other hand, the hydrothermal method has low cost, short cycle, is simple, and can be easily realized and controlled in terms of the reaction conditions.

As electron transport layer material, one-dimensional TiO_2 nanorod films are widely used in photoanodes of new solar cells [16,17]. This structure can reduce the band edge, surface state and crystal defects in films, and can effectively enhance the light scattering effects of the photoanode [18] since the one-dimensional nanomaterial provides a nearly straight transmission path for the electrons. The electron transport distance is shortened, the electrons lifetime is prolonged, the charge recombination is reduced, and the carrier quantum yield is improved, which all lay a foundation for the good photoelectric performance of the solar cells [19]. The premise for achieving this goal is to prepare a one-dimensional TiO_2 nanorod film with perfect structure, morphology, excellent orientation and suitable thickness, which are closely related to the reaction parameters of the hydrothermal reaction.

* Corresponding author.
E-mail address: renfz@haust.edu.cn (F. Ren).

https://doi.org/10.1016/j.cplett.2019.03.054
Received 26 January 2019; Received in revised form 25 March 2019; Accepted 26 March 2019
Available online 27 March 2019

In this paper, stable rutile phase 1D TNA films were successfully prepared on the FTO substrates. Specifically, $TiCl_4$ and $Ti(OC_4H_9)_4$ were used as the titanium sources of TCL and 1D TNA films, respectively, which were different from the previous studies where a single titanium source was often used as the raw material. In addition, the two-step process was adopted to utilize good coordination of the two different titanium sources and successfully prepare the ideal TiO_2 nanomaterials. First, a layer of TCL was deposited as a seed layer on the FTO substrate by thermal deposition using titanium tetrachloride as the titanium source, called FTO_{TCL}. Then, a layer of 1D TNA films as the electron transport layers (ETLs) with perfect crystallization was grown on FTO_{TCL} using a hydrothermal method with tetrabutyl titanate as the titanium source. The materials were characterized by field emission scanning electron microscopy (FESEM), X-ray diffraction (XRD), UV-vis spectroscopy, photoluminescence (PL) spectra experiments, electrochemical impedance spectroscopy (EIS) and transient photocurrent. The effects of TCL and hydrothermal reaction time on the morphology, structure and photoelectric properties of 1D TNA films were studied in detail. The best experimental parameters were determined to provide a reference for the preparation of photovoltaic devices with excellent properties in the future.

2. Experimental section

2.1. Materials

Tetrabutyl titanate [$Ti(OC_4H_9)_4$, ≥98% pure], titanium tetrachloride ($TiCl_4$, ≥98% pure), hydrochloric acid (HCl, 36–38 wt%), anhydrous ethanol (CH_3CH_2OH, ≥99.7%), acetone (CH_3COCH, ≥99.5%) and isopropanol [$(CH_3)_2CHOH$, ≥99.7%] were purchased from the Sinopharm Chemical Reagent Co., Ltd. Deionized water (homemade), F-doped SnO_2 transparent conductive glass (FTO, 30 × 30 × 2.2 mm^3, square resistance ≤ 14 Ω/□, transmittance ≥ 90%) was purchased from the South China Science & Technology Co., Ltd. and used as a substrate. The FTO was washed with acetone, isopropanol, and deionized water before use.

2.2. TiO_2 compact layer synthesis

Under ice water bath conditions, 2.2 mL of $TiCl_4$ were slowly added to 100 mL of cold deionized water (< 3 °C) while stirring, and a small amount of pale-yellow solid was generated in the solution, and a large amount of white smoke appeared. As the stirring progressed, the above phenomena gradually disappeared. After the solution was completely clear and transparent, a 0.2 M aqueous solution of $TiCl_4$ was obtained [12]. After placing the cleaned FTO substrate into the beaker with the conductive surface up, the appropriate amount of aqueous solution of $TiCl_4$ was slowly poured into the beaker to completely immerse the FTO substrate. Then the beaker was sealed and placed in a constant temperature drying oven for 30 min at 70 °C. In the end, the FTO substrate was taken out and rinsed with anhydrous ethanol and deionized water several times, and then the dried FTO substrate was placed in a muffle furnace and annealed at 550 °C for 1 h. A compact layer of TiO_2 (TCL) was obtained on the FTO substrate.

2.3. One-dimensional TiO_2 nanorod array films synthesis

A mixed solution of concentrated hydrochloric acid and deionized water ($HCl:H_2O$ = 2:1, 60 mL) and 1 mL of tetrabutyl titanate were mixed, and then tetrabutyl titanate was slowly added to the aqueous hydrochloric acid solution at a rate of about 1 drop per 3 s. Continued vigorous stirring was required to avoid hydrolysis of tetrabutyl titanate until the solution was clear and transparent. The prepared FTO_{TCL} was placed in a Teflon liner (50 mL) and the FTO_{TCL} was maintained at an angle of 45–60° to the vertical wall. The prepared solution was then poured into the reactor lining and sealed, and the reactor was placed in a constant temperature drying oven at 150 °C for the hydrothermal reaction [20]. After that, the FTO_{TCL} was taken out and washed several times with absolute ethanol and deionized water, and then the dried FTO_{TCL} was annealed in a muffle furnace at 450 °C for 30 min, and then on the FTO_{TCL}. Thus, one-dimensional TiO_2 nanorod array films (1D TNA films) were prepared.

In addition, in order to investigate the effect of the presence or absence of TCL on the performance of 1D TNA films, the same hydrothermal reaction was carried out using bare FTO substrates, and 1D TNA films were also obtained.

2.4. Characterization

The surface morphology and cross-sectional images of the samples were examined by the field-emission scanning electron microscopy (FESEM, JSM-7800 F, JEOL). The X-ray diffraction data were acquired using a Bruker D8 Advance powder X-ray diffractometer (Bruker, Germany), the X-ray tube produced Cu Kα radiation (λ = 1.5406 Å), and the generator was set to 40 kV and 40 mA during the data collection. Data was collected in the 20–80° 2θ angle range. A UV–visible spectrophotometer (UV-2600, Shimadzu) was utilized to obtain the transmittance spectra and absorption spectra of the 1D TNA films. The photoluminescence (PL) spectra experiments were performed using a WFY-28 fluorescence spectrophotometer (Tianjin Tuo Pu Instrument Co., Ltd). EIS measurements were carried out by an electrochemical workstation (CHI660D, Beijing Join Technology Co., Ltd) under the dark condition and at a bias of 0.48 V with the frequency sweeping from 1 Hz to 1 MHz. The spectra were fitted using the ZSimpWin software. The transient photocurrent characteristics were recorded at a cycle of 40 s by using the same electrochemical workstation under simulated AM 1.5G sunlight at 100 mW cm^{-2} irradiation generated by a solar simulator (Solar IV, Beijing Zolix Instruments Co., Ltd), which was calibrated by the 91150-KG5 reference cell (Newport, USA). All samples were measured in the air at 25 °C.

3. Results and discussion

3.1. Morphology and structure

Fig. 1a–e present the FESEM images of 1D TNA films on FTO_{TCL}, and the corresponding hydrothermal reaction time was 6 h, 9 h, 12 h, 15 h, and 18 h, respectively. Fig. 1f is the FESEM image of the 1D TNA film obtained by the hydrothermal reaction on the bare FTO substrate for 15 h. Among them, the main images are the side views of 1D TNA films, and the insert images are the top views of the 1D TNA films. Compared with the 1D TNA film (2.4 μm, Fig. 1f) grown on bare FTO, the 1D TNA film grown on FTO_{TCL} is thicker (3.1 μm in Fig. 1d), and the larger diameter of the TiO_2 nanorods will significantly increase the specific surface area of the film, which can effectively enhance the scattering rate of the film, promote the absorption of light by the photosensitive material in the photoanode, and thereby improve the utilization of sunlight, especially visible light [14]. In addition, the 1D TNA film grown on FTO_{TCL} exhibits better directional growth and perpendicularity, which will help reduce the concentration of crystal defects, reduce the charge recombination center formed by defects, and thus increase the quantum yield of photogenerated carriers. At the same time, the adjacent TiO_2 nanorods are arranged more closely. The dense 1D TNA film and the TCL on the FTO substrate can effectively prevent the direct contact between the FTO conductive layer and the redox electrolyte, thereby reducing the dark current in the solar cells [12]. The factors causing the above differences can be attributed to the difference in nucleation types. The nucleation type of TiO_2 nanorods formed on the bare FTO substrate was the primary nucleation, during which the system contains no substances to be crystallized. Since there was a certain lattice mismatch rate between the TiO_2 crystals and the SnO_2 crystals in the substrate, in this case, if TiO_2 wanted to nucleate and

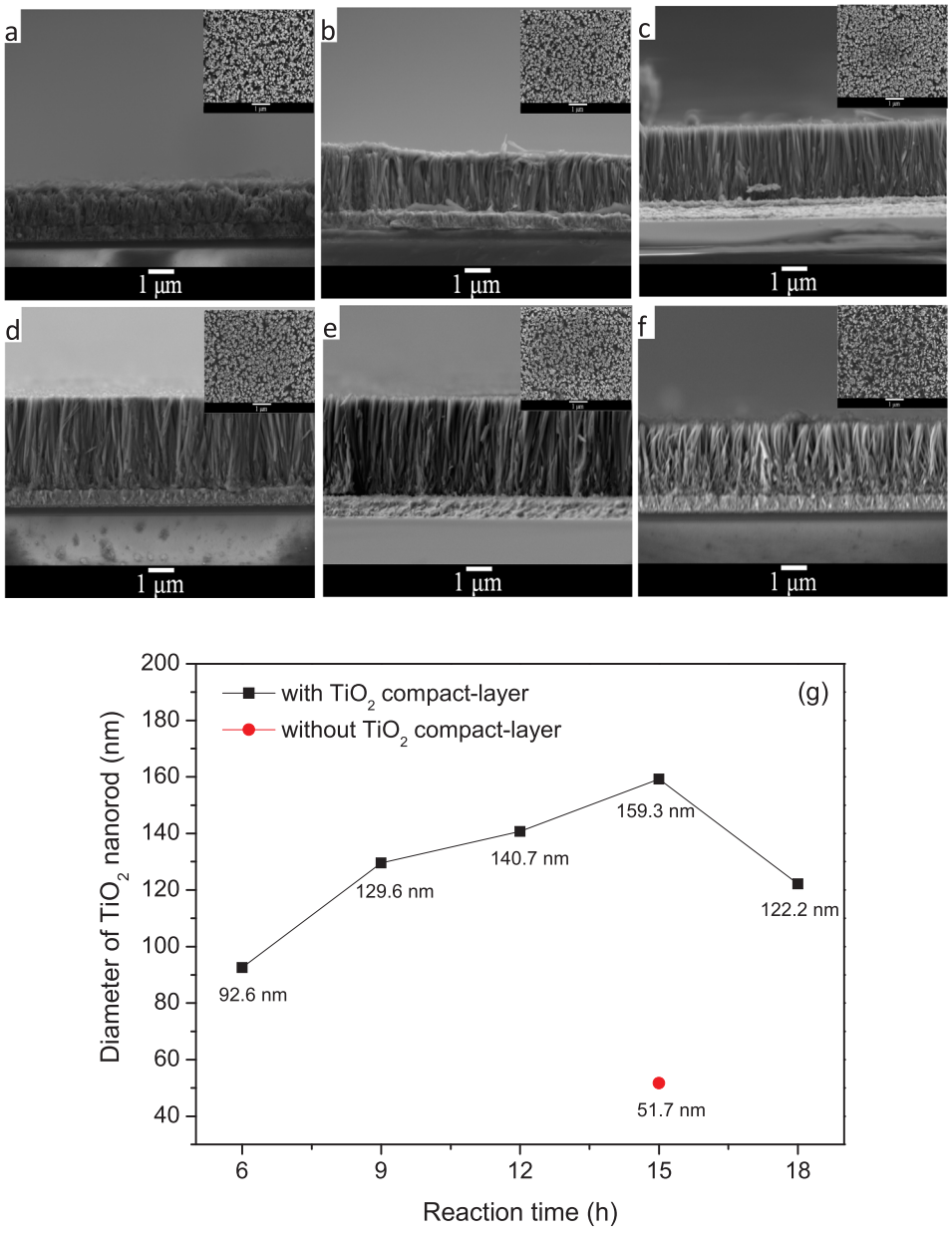

Fig. 1. FESEM images of various 1D TNA films: (a) 6 h, (b) 9 h, (c) 12 h, (d) 15 h, (e) 18 h, (f) without TCL and (g) various diameters of TiO_2 nanorods.

crystallize on the FTO substrate, it was necessary to overcome a large energy barrier caused by lattice mismatch, which will have a certain impact on the growth process of TiO_2 nanorods. In contrast, the nucleation type of TiO_2 nanorods formed on the FTO_{TCL} substrate belonged to secondary nucleation. During nucleation, substances in the system that have been waiting for crystallization were contained. Since there was no lattice mismatch, it was easier for TiO_2 to nucleate and crystallize on the FTO_{TCL} substrate. Therefore, the different nucleation types of TiO_2 on different substrates resulted in different morphology of TiO_2 nanorods.

Fig. 1a–e show that based on FTO_{TCL}, changing the hydrothermal reaction time has a significant effect on the morphology of 1D TNA films. From 6 h (1.5 μm in Fig. 1a) to 9 h (2.1 μm in Fig. 1b), both the thickness of the 1D TNA films and the diameter of the TiO_2 nanorods increased significantly. Compared with the disordered packing arrangement of TiO_2 nanorods in Fig. 1a and the lower density of 1D TNA film in top view, although the tip of TiO_2 nanorods in Fig. 1b exhibits a curved growth phenomenon, the directional growth of TiO_2 nanorods and the verticality, and the density of the 1D TNA film in the top view have been improved. This result shows that prolonging the hydrothermal reaction time can effectively improve the crystallization characteristics of TiO_2 and better promote directional crystal growth. It will be beneficial for the overall performance improvement of the 1D TNA films.

The above results were further verified by increasing the hydrothermal reaction time to 12 h (2.5 μm in Fig. 1c), 15 h (3.1 μm in Fig. 1d) and 18 h (3.3 μm in Fig. 1e). At this point, the TiO_2 nanorods in Fig. 1c-e have fully achieved vertical orientation growth, which is greatly improved compared to the verticality of the TiO_2 nanorods in Fig. 1a and b, and the 1D TNA films in the top views are also more uniform and denser. Compared with Fig. 1d (3.1 μm, 15 h), although the thickness of the 1D TNA film in Fig. 1e (3.3 μm, 18 h) is 0.2 μm larger, there is already a small difference between the bottom of the 1D TNA film and the FTO_{TCL} substrate. The appearance of this difference will affect the degree of bonding of the 1D TNA film to the FTO_{TCL} substrate and may even cause the 1D TNA film to fall off the FTO_{TCL} substrate, thereby weakening or eliminating the performance advantages of the 1D TNA film. In addition, the tightness of alignment

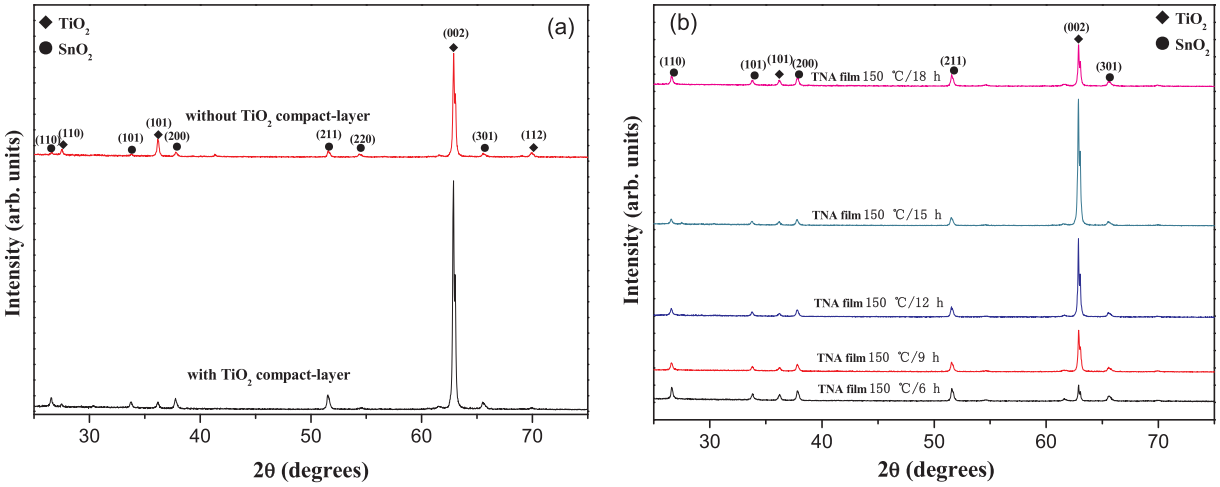

Fig. 2. XRD patterns of various 1D TNA films: (a) with or without TCL and (b) various reaction times.

between adjacent TiO_2 nanorods in Fig. 1e is reduced, the quadrangular prism shape of TiO_2 nanorods becomes irregular, and the smoothness and flatness of the sides of TiO_2 nanorods are also reduced. These changes will ultimately have a negative impact on the performance of 1D TNA films and later fabricated components. Similarly, the effects of TCL and various hydrothermal reaction times on the diameters of TiO_2 nanorods were shown in Fig. 1g. The presence of TCL increased the diameters of TiO_2 nanorods by 3.1 times, from 51.7 nm to 159.3 nm. With the change of hydrothermal reaction time, the diameters of TiO_2 nanorods reached the maximum at 15 h. The increase of the diameters of TiO_2 nanorods greatly increased the specific surface area of 1D TNA films, and significantly increased the effective adsorption amount of photosensitive materials, enhancing the light absorption of 1D TNA films and improving the quantum yield of photogenerated carriers.

Fig. 2a is an XRD pattern of a 1D TNA film grown on a bare FTO substrate (without TCL) and a 1D TNA film grown on an FTO_{TCL} substrate (with TCL). The diffraction reflections at 2θ = 27.54°, 36.22°, 62.93° and 69.97° in the pattern correspond to the (1 1 0), (1 0 1), (0 0 2) and (1 1 2) crystal planes of the rutile TiO_2 crystal, respectively, and the results are compared with the standard XRD pattern (JCPDS 65-192 #). The remaining diffraction reflections originate from the FTO substrate (JCPDS 77-452 #) [21]. This XRD pattern shows that the diffraction intensity of the (0 0 2) crystal plane is the highest in all TiO_2 crystal diffraction reflections, regardless of the presence or absence of TCL on the FTO substrate. This indicates that the TiO_2 crystals do crystallize along the normal direction of the specific crystal plane, which is also the most important factor for the formation of TiO_2 nanorods. This conclusion is also consistent with the results of the directional growth of TiO_2 nanorods in Fig. 1. At the same time, the intensity of the diffraction peak of the (0 0 2) crystal plane of the 1D TNA film grown on the FTO_{TCL} substrate is remarkably enhanced compared with the 1D TNA film grown on the bare FTO substrate, and the diffraction intensity of other crystal planes becomes very weak or even disappears. This is because TCL acts as a seed layer of TiO_2, which reduces the adverse effect of TiO_2 crystal and FTO due to the large lattice mismatch ratio on the crystal growth of TiO_2 so that TiO_2 crystal can be a good implementation of directional epitaxial crystal growth based on TCL. In addition, the intensity of the diffraction peaks of the FTO substrate is significantly weakened or disappeared, indicating that the TCL deposited on the FTO surface achieves uniform coverage of the FTO surface and acts as a dense layer [22–24].

Based on the FTO_{TCL}, the XRD pattern of the 1D TNA films obtained by changing the hydrothermal reaction time is shown in Fig. 2b. The diffraction peaks of the clearly identifiable rutile TiO_2 crystals in the figure are only the diffraction peaks of the (1 0 1) and (0 0 2) crystal planes, corresponding to 2θ = 36.22° and 62.93°. Compared with other crystal planes of the TiO_2 crystal, TCL has a significant effect on the directional growth of TiO_2 crystal along the normal direction of the (0 0 2) crystal plane. This is equivalent to suppressing the crystal growth of other crystal faces, so in the XRD pattern, only the (0 0 2) crystal plane has a strong diffraction intensity, and the diffraction of other crystal planes is weak or even disappears. As shown in the figure, as the hydrothermal reaction time increases, the intensity of the diffraction peak of the (0 0 2) plane first increases and then decreases. The intensity of the diffraction peak is the strongest at the reaction time of 15 h, and at 18 h the diffraction intensity is significantly lowered. In fact, the crystal growth of TiO_2 crystals during the hydrothermal reaction is a dynamic process involving the crystallization of TiO_2 crystals and the dissolution of TiO_2 crystals. On the one hand, due to the action of TCL, when the hydrothermal reaction time increases from 6 h to 15 h, the intensity of the diffraction reflection of the (0 0 2) crystal plane continues to increase remarkably. On the other hand, with the increase of the hydrothermal reaction time, the reactants in the reaction solution were fully and effectively utilized, and at this time, the crystallization process of the TiO_2 crystal is dominant, so that the TiO_2 crystal can be continuously subjected to directional crystal growth, so that the thickness of the 1D TNA films is continuously increased. This conclusion also corresponds well with the test results of Fig. 1. When the hydrothermal reaction time reaches 18 h, the intensity of the diffraction peak of the (0 0 2) crystal plane is significantly reduced. This is because, after a long period of reaction, the lower concentration of reactants in the reaction solution could not maintain the existing crystallization dynamic equilibrium process. Therefore, the system had to establish a new dynamic equilibrium through the dissolution of TiO_2 crystals. Due to the dissolution of the TiO_2 crystal, as shown in Fig. 1e, a small difference is formed between the bottom of the 1D TNA film and the FTO_{TCL} substrate, and the tightness of the alignment between adjacent TiO_2 nanorods is lowered, and the quadrangular prism shape of the TiO_2 nanorods becomes irregular.

3.2. Optical performance

As shown in Fig. 3, the optical properties of the obtained 1D TNA films were characterized in UV–vis spectra. First, the influence of the presence or absence of TCL on the light absorption intensity of 1D TNA films (Fig. 3a) and its corresponding optical band gap E_g-$(\alpha h\nu)^2$ curve (Fig. 3b) were analyzed. Then, based on the FTO_{TCL}, the effects of changing the hydrothermal reaction time on the light absorption intensity of 1D TNA films (Fig. 3c) and its corresponding optical band gap E_g-$(\alpha h\nu)^2$ curve (Fig. 3d) were studied. In Fig. 3a, the absorbance of the 1D TNA film grown on an FTO_{TCL} is significantly reduced compared to the 1D TNA film grown on a bare FTO, which means that light

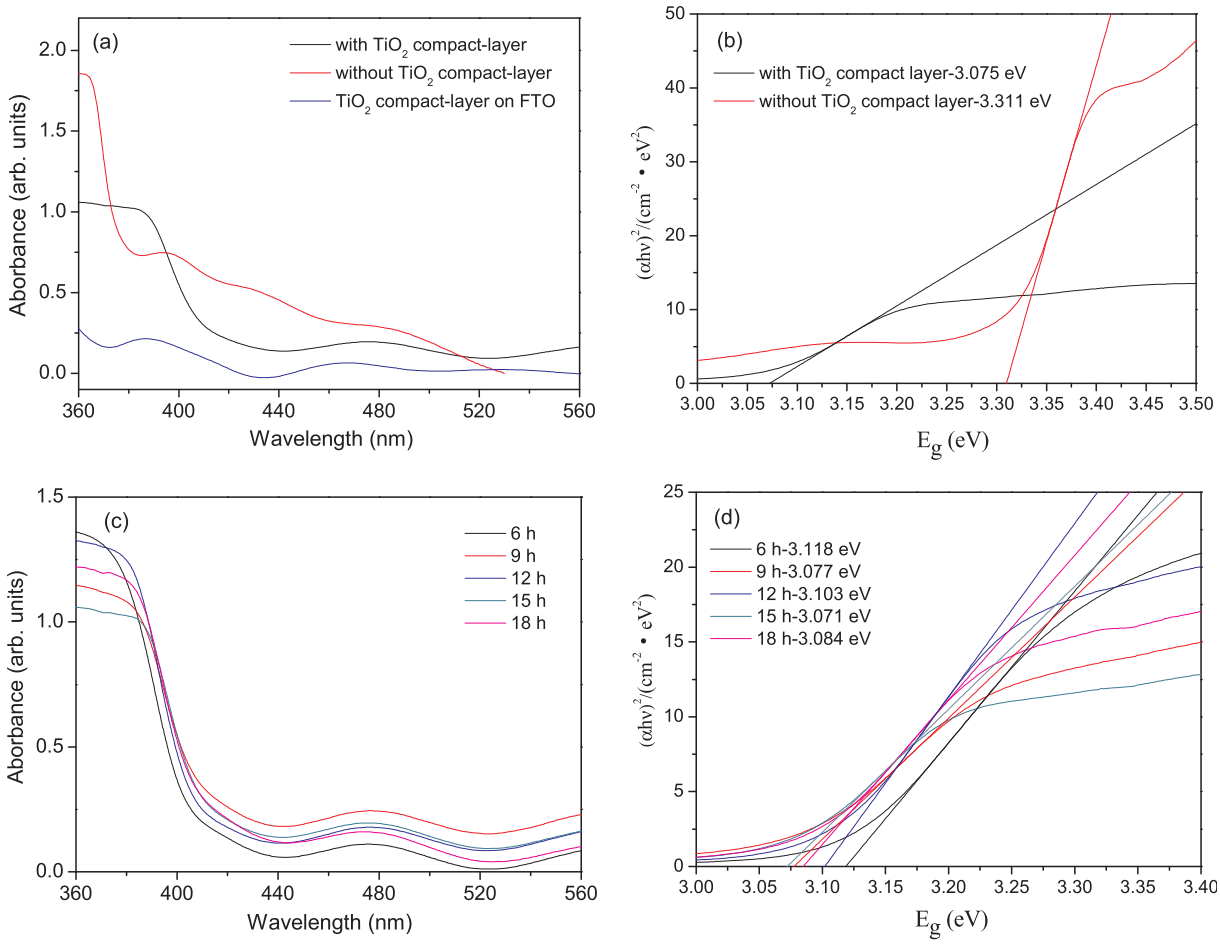

Fig. 3. (a), (c) Absorption spectra and (b), (d) $E_g - (\alpha h\nu)^2$ curve of various 1D TNA films.

transmittance of the 1D TNA film is increased so that more light can be absorbed by the photosensitive material in the photoanode. With the apparent red-shift of the light absorption band edge (from 375 nm to 403 nm), the corresponding optical band gap E_g (Fig. 3b) is also reduced from 3.311 eV to 3.075 eV, the photogenerated electrons produced by the photosensitive material are more easily injected into the conduction band of TiO_2 [25], thereby broadening the effective light absorption range of the photosensitive material, especially enhancing the utilization of visible light.

Based on the FTO_{TCL}, the change in hydrothermal reaction time also affected the light absorption intensity of the 1D TNA films (Fig. 3c). As the hydrothermal reaction time increases, the light absorption intensity of the 1D TNA films in the ultraviolet region ($\lambda < 380$ nm) is significantly reduced, and the transmittance of the corresponding 1D TNA films in the ultraviolet region is significantly increased. In the visible light region ($\lambda > 400$ nm), although the overall light absorption intensity is not high, the light absorption intensity is still increased. However, due to the small increase, the hydrothermal reaction time has a limited effect on the transmittance of 1D TNA films in the visible region. In addition, the light absorption band edge of 1D TNA films also produces a small red-shift with the increase of hydrothermal reaction time, from the smallest 398 nm at 6 h to the maximum 405 nm at 15 h, and the corresponding optical band gap E_g (Fig. 3d) is reduced from 3.118 eV to 3.071 eV, which significantly enhances the efficiency of sunlight utilization.

The photoluminescence spectra are commonly used to characterize electronic structures and electronic states in semiconductor materials. In Fig. 4 the excitation wavelength is 320 nm. Either 1D TNA films grown on the FTO substrate with or without TCL (Fig. 4a), or 1D TNA films grown on FTO_{TCL} with various hydrothermal reaction time (Fig. 4b), their PL spectra are very similar, indicating that the energy level distribution of the TiO_2 crystals in all 1D TNA films does not change significantly, and the distribution of the electronic density of TiO_2 crystals in the band gap is also similar [26]. As shown in Fig. 4a, the fluorescence intensity of the 1D TNA film grown on the FTO_{TCL} was significantly reduced compared to the 1D TNA film grown on the bare FTO. The reason is that TCL can promote better crystal growth of TiO_2 crystals, thereby reducing defects in TiO_2 crystals [27], which cause the number of charge recombination centers to decrease, and electrons and holes are effectively separated. Since the charge recombination rate is lowered, the intensity of fluorescence generated by charge recombination is lowered. As shown in Fig. 4b, as the hydrothermal reaction time increases, the fluorescence intensity of 1D TNA films decreases first and then increases, and the fluorescence intensity is the weakest at 15 h. The reason is similar to the analysis results of Fig. 2b. The increase of the hydrothermal reaction time makes the reactants in the reaction solution fully utilized, and the formed TiO_2 crystal is also more perfect with fewer crystal defects, so the recombination of electrons and holes at the charge recombination centers is reduced, resulting in a decrease in fluorescence intensity. When the hydrothermal reaction time reaches 18 h, the dissolution process of TiO_2 crystals dominates because of the concentration of reactants in the reaction solution being too low [28]. The dissolution of TiO_2 crystal not only destroys the appearance of the crystal, but also has a certain negative influence on the internal structure of the crystal, and even increases the crystal defects, resulting in an increase in the recombination rate of the charges, which makes the fluorescence intensity significantly enhanced. In addition, according to the position and intensity analysis of the PL

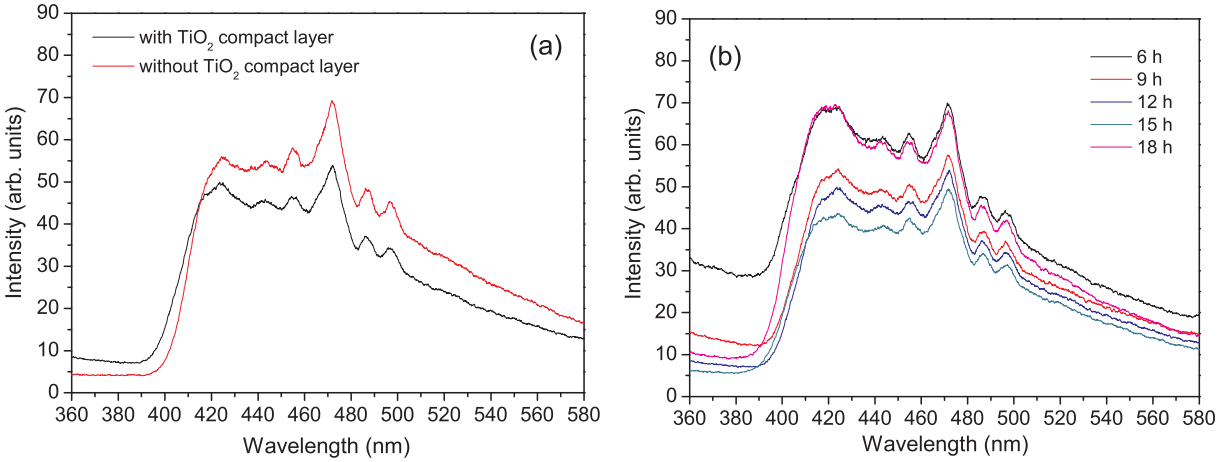

Fig. 4. PL spectra of various 1D TNA films: (a) with or without TCL and (b) various reaction times.

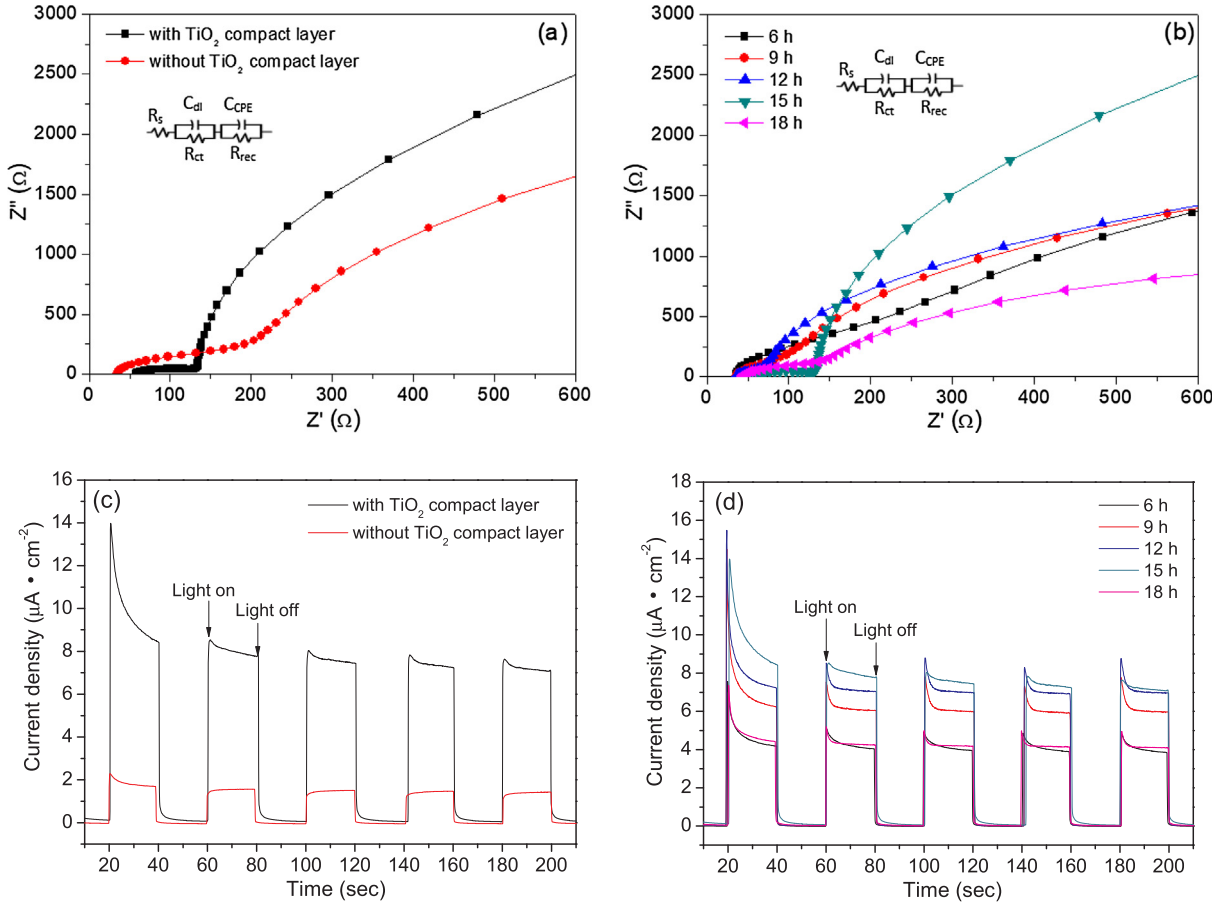

Fig. 5. (a), (b) Nyquist plots and (c), (d) transient photocurrent spectra of various 1D TNA films.

Table 1
Fitting results of the Nyquist plots.

Samples	R_s (Ω)	R_{ct} (Ω)	R_{rec} (kΩ)
6 h (with TCL)	43.22	5.21	13.96
9 h (with TCL)	57.65	6.75	22.13
12 h (with TCL)	28.17	7.91	32.15
15 h (with TCL)	35.58	4.21	43.73
18 h (with TCL)	43.35	55.35	12.05
15 h (without TCL)	34.92	182.63	41.42

peaks, the PL peak at 423.5 nm is the bound exciton peak, and the intensity is weak. The latter two PL peaks at 443.5 nm and 455 nm are phonon peaks. The sharp PL peak at 471.5 nm is a free exciton peak with strong intensity. The latter two PL peaks at 486.5 nm and 496.5 nm are also phonon peaks [29].

3.3. Electrical properties

EIS is commonly used to characterize the dynamic properties of electrons in a film, including the transfer of charge between different interfaces and the recombination of charges. The Nyquist plots of the

different 1D TNA films are shown in Fig. 5a and b, and the fitting results of the Nyquist plots are listed in Table 1. EIS was performed from 1 Hz to 1 MHz under dark conditions at a bias voltage of 0.48 V. In the EIS equivalent analog circuit, R_s, R_{ct}, and R_{rec} represent the solution resistance between the working electrode and the electrolyte, charge transfer resistance and charge recombination resistance [30,31]. R_{ct} and R_{rec} correspond to small arcs in the high-frequency region and large arcs in the low-frequency region of the Nyquist plots, respectively. In Fig. 5a, the 1D TNA film with TCL has a smaller curvature compared to the 1D TNA film without TCL, and the corresponding R_{ct} is reduced from 182.63 Ω to 4.21 Ω. The curvature of the large arc is larger, and the corresponding R_{rec} increases from 41.42 kΩ to 43.73 kΩ. The decrease of R_{ct} and the increase of R_{rec} indicate that the presence of TCL not only makes the 1D TNA film have better charge transport performance but also can effectively prevent the recombination of charges and make the charge recombination more difficult. These have a positive effect on improving the electrical performance of 1D TNA films. Based on the FTO_{TCL}, as shown in Fig. 5b, with the increase of hydrothermal reaction time, the Nyquist plots obtained the minimum arc curvature and the maximum arc curvature in the low-frequency region and the high-frequency region at 15 h, respectively. The corresponding minimum R_{ct} and the maximum R_{rec} are 4.21 Ω and 43.73 kΩ, respectively, indicating that the 1D TNA film obtained at 15 h hydrothermal reaction has better charge transport and lower charge recombination rate. The reason is similar to the analysis results in Fig. 2b. Increasing the time of hydrothermal reaction within a certain range can promote better crystallization of TiO_2, but the reaction time is too long, which causes the dissolution of the TiO_2 crystal, which not only destroys the structure of the TiO_2 crystal but also causes more crystal defects.

To further investigate the electrical properties of 1D TNA films, the transient photocurrent spectra of various 1D TNA films measured at 0.5 M Na_2SO_4 solution and 0 V potential (calomel electrode) are shown in Fig. 5c and d [32]. Compared with the 1D TNA film without TCL, the transient photocurrent of the 1D TNA film with TCL is significantly higher (Fig. 5c). As the hydrothermal reaction time increases, the transient photocurrent intensity also increases and reaches a maximum at 15 h, after which the transient photocurrent decreases at 18 h (Fig. 5d). This result can be explained by the generation-separation-recombination mechanism of photogenerated carriers [33]. In the 1D TNA film with TCL, even if the total quantum yield of the photogenerated carriers is constant, the crystallization of the TiO_2 crystal is better, the crystal structure is more ideal with fewer crystal defects. The charge transport performance of the 1D TNA film is better, the charge recombination rate is lower so that more electrons and holes are effectively separated, and the effective charge concentration is increased to form a higher current. Similarly, appropriately increasing the hydrothermal reaction time promotes the crystallization of TiO_2 and improves the vertical orientation of TiO_2 nanorods, which not only reduces the concentration of defects in the crystal, reduces the charge recombination, makes more electrons and holes effectively separated, but also provides a faster linear transmission path for the photogenerated electrons, thereby accumulating more charge and increasing the current on the electrodes.

4. Conclusions

The rutile 1D TNA films were successfully prepared on bare FTO and FTO_{TCL} by thermal deposition and hydrothermal methods. TCL also acts as a seed layer of TiO_2 while improving the compactness of the film, which effectively reduces the lattice mismatch between FTO and TiO_2 crystals. 1D TNA film with TCL enhances the use of visible light, reduces defects in TiO_2 crystals, reduces the charge recombination center caused by defects, effectively separates electrons and holes, and reduces charge recombination rate, so that the film has better charge transfer performance, and transient photocurrents increase significantly. When the reaction time is 15 h, the TiO_2 crystal has better crystallinity and fewer crystal defects, while the reduction of optical band gap E_g can significantly enhance the utilization efficiency of sunlight, therefore, the better charge transfer and the ability to prevent charge recombination of the 1D TNA film maximizes the transient photocurrent.

Acknowledgments

This work was supported by the Chinese Postdoctoral Science Fund (2343/185179), the Chinese 02 Special Fund (2017ZX02408003), the Key Research Projects of Colleges and Universities in Henan province (15A430023) and the Henan International Science and Technology Cooperation Programs (152102410035).

References

[1] Y. Zhang, N. Zhou, K. Zhang, F. Yan, Plasmonic copper nanowire@TiO_2 nanostructures for improving the performance of dye-sensitized solar cells, J. Power Sources 342 (2017) 292–300.
[2] R.S. Dubey, Temperature-dependent phase transformation of TiO_2 nanoparticles synthesized by sol-gel method, Mater. Lett. 215 (2018) 312–317.
[3] Q.H. Liu, Q. Sun, M. Zhang, Y. Li, M. Zhao, L.F. Dong, Enhanced photoelectrical performance of dye-sensitized solar cells with double-layer TiO_2 on perovskite $SrTiO_3$ substrate, Appl. Phys. A: Mater. 122 (2016) 1–5.
[4] X. Tong, W.H. Shen, X.Q. Chen, Enhanced H_2S sensing performance of cobalt doped free-standing TiO_2 nanotube array film and theoretical simulation based on density functional theory, Appl. Surf. Sci. 469 (2019) 414–422.
[5] M.C. Wu, P.Y. Wu, T.H. Lin, T.F. Lin, Photocatalytic performance of Cu-doped TiO_2 nanofibers treated by the hydrothermal synthesis and air-thermal treatment, Appl. Surf. Sci. 430 (2018) 390–398.
[6] Y.B. Chen, X.M. Li, Z.J. Bi, X.L. He, G.J. Li, X.K. Xu, X.D. Gao, Design and construction of hierarchical TiO_2 nanorod arrays by combining layer-by-layer and hydrothermal crystallization techniques for electrochromic application, Appl. Surf. Sci. 440 (2018) 217–223.
[7] S. Mathew, A. Yella, P. Gao, R. Humphry-Baker, B.F.E. Curchod, N. Ashari-Astani, I. Tavernelli, U. Rothlisberger, Md.K. Nazeeruddin, M. Grätzel, Dye-sensitized solar cells with 13% efficiency achieved through the molecular engineering of porphyrin sensitizers, Nat. Chem. 6 (3) (2014) 242–247, https://doi.org/10.1038/nchem.1861.
[8] C. Liang, P. Li, Y. Zhang, H. Gu, Q.B. Cai, X.T. Liu, J.F. Wang, H. Wen, G.S. Shao, Mild solution-processed metal-doped TiO_2 compact layers for hysteresis-less and performance-enhanced perovskite solar cells, J. Power Sources 372 (2017) 235–244.
[9] O. Krško, T. Plecenik, T. Roch, B. Grančič, L. Satrapinskyy, M. Truchlý, P. Ďurina, M. Gregor, P. Kúš, A. Plecenik, Flexible highly sensitive hydrogen gas sensor based on a TiO_2 thin film on polyimide foil, Sensor. Actuat. B: Chem. 240 (2017) 1058–1065.
[10] R. Bashiri, N.M. Mohamed, C.F. Kait, S. Sufiana, M. Khatanib, H. Hanaei, Effect of preparation parameters on optical properties of Cu and Ni doped TiO_2 photocatalyst, Procedia Eng. 148 (2016) 151–157.
[11] R. Sivakumar, J. Ramkumar, S. Shaji, M. Paulra, Effect of TiO_2 blocking layer on TiO_2 nanorod arrays-based dye sensitized solar cells, Energy Procedia 615 (2016) 171–176.
[12] R. Govindaraj, N. Santhosh, M.S. Pandian, P. Ramasamy, Synthesis of nanocrystalline TiO_2 nanorods via hydrothermal method: an efficient photoanode material for dye sensitized solar cells, J. Cryst. Growth 468 (2017) 125–128.
[13] B.B. Çırak, S.M. Karadeniz, T. Kılınç, B. Caglar, A.E. Ekinci, H. Yelgin, M. Kürekçi, Ç. Çırak, Synthesis, surface properties, crystal structure and dye sensitized solar cell performance of TiO_2 nanotube arrays anodized under different voltages, Vacuum 144 (2017) 183–189.
[14] N. Nyein, W.K. Tan, G. Kawamura, A. Matsuda, Z. Lockman, TiO_2 nanotube arrays formation in fluoride/ethylene glycol electrolyte containing LiOH or KOH as photoanode for dye-sensitized solar cell, J. Photoch. Photobio. A 343 (2017) 33–39.
[15] N. Sriharan, N. Muthukumarasamy, T.S. Senthil, M. Kang, Preparation of dye-sensitized solar cells using template free TiO_2 nanotube arrays for enhanced power conversion, J. Sol-Gel Sci. Technol. 85 (2018) 743–752.
[16] B. Rezaei, I. Mohammadi, A.A. Ensafi, Mohammad M Momeni, Enhanced efficiency of DSSC through AC-electrophoretic hybridization of TiO_2 nanoparticle and nanotube, Electrochim. Acta 247 (2017) 410–419.
[17] S.S. Kim, S.I. Na, Y.C. Nah, TiO_2 nanotubes decorated with ZnO rod-like nanostructures for efficient dye-sensitized solar cells, Electrochim. Acta 58 (2011) 503–509.
[18] J. Liu, J. Huo, M. Zhang, X.D. Dong, Branched TiO_2 nanorod arrays owning the surface anatase/rutile junctions for dye sensitized solar cells, Thin Solid Films 623 (2017) 25–30.
[19] D. Jiang, Y. Hao, R. Shen, S. Ghazarian, A. Ramos, F.M. Zhou, Effective blockage of the interfacial recombination process at TiO_2 nanowire array electrodes in dye-sensitized solar cells, ACS Appl. Mater. Inter. 5 (2013) 11906–11912.
[20] B. Liu, E.S. Aydil, Growth of oriented single-crystalline rutile TiO_2 nanorods on transparent conducting substrates for dye-sensitized solar cells, J. Am. Chem. Soc. 131 (2009) 3985–3990.
[21] Y.F. Deng, X.L. Li, Z.H. Ma, X.L. Ming, F.Z. Ren, Morphology and optical properties

of one-dimensional single crystal TiO_2 nanorods thin film, Semicond. Optoelectron. 39 (2018) 836–842.
[22] H. Yu, S.Q. Zhang, H.J. Zhao, G. Will, P. Liu, An efficient and low-cost TiO_2 compact layer for performance improvement of dye-sensitized solar cells, Electrochim. Acta 54 (2009) 1319–1324.
[23] M.S. Wu, C.H. Tsai, T.C. Wei, Anodic deposition of ultrathin TiO_2 film with blocking layer and anchoring layer for dye-sensitized solar cells, J. Electrochem. Soc. 159 (2012) B81–B86.
[24] V Saxena Tanvi, A. Singh, O. Prakash, A. Mahajan, A.K. Debnath, K.P. Muthe, S.C. Gadkari, Improved performance of dye sensitized solar cell via fine tuning of ultrathin compact TiO_2 layer, Sol. Energ. Mat. Sol. C. 170 (2017) 127–136.
[25] Y. Lv, Y. Li, H. Sun, Y. Guo, Y.M. Li, J.K. Tan, X.F. Zhou, Yttrium-doped TiO_2 nanorod arrays and application in perovskite solar cells for enhanced photocurrent density, Thin Solid Films 651 (2018) 117–123.
[26] W.L. Xu, H. Yuan, J. Xiao, C. Xiong, X.F. Zhu, Morphology, photophysics and optoelectronics of P3HT nanoparticles and TiO_2 nanorods composite, Int. J. Mod. Phys. B 31 (2017).
[27] P. Vivo, A. Ojanpera, J.H. Smått, S. Sanden, S.G. Hashmi, K. Kaunisto, P. Ihalainen, M.T. Masood, R. Osterbacka, P.D. Lund, H. Lemmetyinen, Influence of TiO_2 compact layer precursor on the performance of perovskite solar cells, Org. Electron. 41 (2017) 287–293.
[28] D. Tang, K. Cheng, W. Weng, C.L. Song, P.Y. Du, G. Shen, G.R. Han, TiO_2 nanorod films grown on Si wafers by a nanodot-assisted hydrothermal growth, Thin Solid Films 519 (2011) 7644–7649.
[29] M.A. Alvi, A.A. Alghamdi, M. Zulfequar, Synthesis and characterization of cadmium chalcogenide semiconductor quantum dots based thin film, J. Nanoelectron. Optoe. 11 (2016) 656–661.
[30] X.Y. Liu, Z.Y. Liu, B. Sun, X.H. Tan, H.B. Ye, Y.X. Tu, T.L. Shi, Z.R. Tang, G.L. Liao, All low-temperature processed carbon-based planar heterojunction perovskite solar cells employing Mg-doped rutile TiO_2 as electron transport layer, Electrochim. Acta 283 (2018) 1115–1124.
[31] S. Wang, B. Liu, Y. Zhu, Z.R. Ma, B.B. Liu, X. Miao, R.X. Ma, C.Y. Wang, Enhanced performance of TiO_2-based perovskite solar cells with Ru-doped TiO_2 electron transport layer, Sol. Energy 169 (2018) 335–342.
[32] J.T. Li, J.P. McClure, R. Fu, R.Z. Jiang, D. Chu, Understanding charge transfer dynamics in QDs-TiO_2 nanorod array photoanodes for solar fuel generation, Appl. Surf. Sci. 429 (2018) 48–54.
[33] H. Wang, Y. Bai, H. Zhang, Z.H. Zhang, J.H. Li, L. Guo, CdS quantum dots-sensitized TiO_2 nanorod array on transparent conductive glass photoelectrodes, J. Phys. Chem. C 114 (2010) 16451–16455.